



This is a repository copy of *Ultrafast exciton and trion dynamics in high-quality encapsulated MoS2 monolayers*.

White Rose Research Online URL for this paper:

<https://eprints.whiterose.ac.uk/192564/>

Version: Published Version

Article:

Genco, A., Trovatiello, C., Louca, C. et al. (5 more authors) (2023) Ultrafast exciton and trion dynamics in high-quality encapsulated MoS2 monolayers. *physica status solidi (b)*, 260 (5). 2200376. ISSN 0370-1972

<https://doi.org/10.1002/pssb.202200376>

Reuse

This article is distributed under the terms of the Creative Commons Attribution (CC BY) licence. This licence allows you to distribute, remix, tweak, and build upon the work, even commercially, as long as you credit the authors for the original work. More information and the full terms of the licence here:

<https://creativecommons.org/licenses/>

Takedown

If you consider content in White Rose Research Online to be in breach of UK law, please notify us by emailing eprints@whiterose.ac.uk including the URL of the record and the reason for the withdrawal request.



eprints@whiterose.ac.uk
<https://eprints.whiterose.ac.uk/>

Ultrafast Exciton and Trion Dynamics in High-Quality Encapsulated MoS₂ Monolayers

Armando Genco,* Chiara Trovatiello, Charalambos Louca, Kenji Watanabe, Takashi Taniguchi, Alexander I. Tartakovskii, Giulio Cerullo, and Stefano Dal Conte*

The extreme confinement and reduced screening in monolayer transition metal dichalcogenides (TMDs) leads to the appearance of tightly bound excitons which can also couple to free charges, forming trions, owing to strong Coulomb interactions. Low temperatures and encapsulation in hexagonal boron nitride (hBN) can narrow the excitonic linewidth, approaching the regime of homogeneous broadening, mostly dominated by the radiative decay. Ultrafast spectroscopy is a perfect tool to study exciton formation and relaxation dynamics in TMD monolayers. However, high-quality hBN-encapsulated structures have usually lateral sizes of the order of a few micrometers, calling for the combination of high spatial and temporal resolution in pump–probe experiments. Herein, a custom broadband pump–probe optical microscope is used to measure the ultrafast dynamics of neutral and charged excitons in high-quality hBN-encapsulated monolayer MoS₂ at 8 K. Neutral excitons exhibit a narrow linewidth of 7.5 meV, approaching the homogeneous limit, which is related to the fast recombination time of ≈ 130 fs measured in pump–probe. Moreover, markedly different dynamics of the trions over the neutral ones are observed. The results provide novel insights on the exciton recombination processes in TMD monolayers, paving the way for exploring the ultrafast behavior of excitons and their many-body complexes in TMD heterostructures.

1. Introduction

Monolayers of transition metal dichalcogenides (1L-TMDs) are promising semiconductors with unique electrical and optical properties. The quantum confinement experienced by electrons and holes in the 2D structure and the reduced Coulomb screening lead to the appearance of direct bandgap excitonic transitions showing high binding energies (up to 0.5 eV) and very large oscillator strengths up to room temperature.^[1–3] Moreover, the breaking of spatial inversion symmetry in the 2D lattice and the large spin–orbit coupling generate spin-valley locked excitons at the K and K' valleys, optically addressable by circularly polarized light.^[4] The strong Coulomb interactions in atomically thin TMDs also enhance the stability of many-body complexes resulting from the correlations of excitons with charge carriers. In this case, TMD excitons are dressed by a Fermi sea of free charges generated in the material by natural or artificial doping, forming three-particle bound states (trions)

in the presence of low doping levels, or manifesting emerging many-body phenomena at elevated doping regimes.^[5–7]


1Ls TMDs also offer the tremendous advantage of being stackable to form van der Waals heterostructures (HSs), with atomically perfect interfaces without any lattice mismatch limitation.^[8] This allows to sandwich the 1Ls between few-layers of transparent high bandgap hexagonal boron nitride (hBN), ensuring a good protection from external contaminants and dielectric insulation. hBN encapsulation has proven to be a key requirement for obtaining good optical quality from small flakes of mechanically exfoliated TMD 1Ls.^[9,10] Cryogenic temperatures and encapsulation in hBN narrow the exciton lines,^[11] reaching the homogeneous linewidth regime, in which the dephasing rate is dominated by radiative recombination.^[12] The high quality of encapsulated TMDs reveals a Rydberg series of excitonic states below the free particle bandgap, which has been previously shown to be slightly nonhydrogenic.^[13] In addition, the encapsulation of TMD bilayers recently allowed to unveil hybridized intra–inter layer excitonic species,^[14,15] showing new types of many-body interactions.^[16]

Femtosecond pump–probe spectroscopy^[17–19] is a powerful technique to measure the temporal dynamics of excitons in 1L

A. Genco, C. Trovatiello,^[†] G. Cerullo, S. Dal Conte
Dipartimento di Fisica
Politecnico di Milano
20133 Milano, MI, Italy
E-mail: armando.genco@polimi.it; stefano.dalconte@polimi.it

C. Louca, A. I. Tartakovskii
Department of Physics and Astronomy
University of Sheffield
Sheffield S3 7RH, UK

K. Watanabe, T. Taniguchi
Advanced Materials Laboratory
National Institute for Materials Science
1-1 Namiki, Tsukuba 305-0044, Japan

 The ORCID identification number(s) for the author(s) of this article can be found under <https://doi.org/10.1002/pssb.202200376>.

^[†]Present address: Department of Mechanical Engineering, Columbia University, New York, NY 10027, USA

© 2022 The Authors. physica status solidi (b) basic solid state physics published by Wiley-VCH GmbH. This is an open access article under the terms of the Creative Commons Attribution License, which permits use, distribution and reproduction in any medium, provided the original work is properly cited.

DOI: 10.1002/pssb.202200376

TMDs. Using this technique, the photoinduced modifications of the excitonic absorption spectrum are monitored in real time. In this way, a full picture of the exciton dynamics is revealed, observing in particular their build-up and decay times. The non-equilibrium optical response of neutral and charged excitons in TMDs has been previously investigated by ultrafast optical spectroscopy, focusing the study on the fundamental mechanisms that determine exciton formation,^[20] dissociation, and decay processes.^[21] However, very few works studied in detail the ultrafast dynamics of TMD excitons and their many-body complexes in small area encapsulated samples because achieving simultaneously a good temporal and spatial resolution in pump-probe experiments is challenging.

In this work, we study the nonequilibrium optical response in hBN-encapsulated monolayer MoS₂, with very narrow excitonic linewidths, approaching the homogeneous broadening regime. We develop a custom pump-probe microscopy setup with high spatial and temporal resolution, broad spectral coverage, and pump energy tunability, which allows us to study samples with lateral size of few micrometers, performing full static and transient optical characterizations. Pumping the system above the bandgap, the neutral excitons reveal distinct dynamics characterized by an ultrafast formation, a fast decay, which we ascribe to direct recombination processes, and a slower one, related to carrier cooling. Trions are also observed in the sample due to residual natural doping, showing different formation and relaxation dynamics compared to neutral excitons.

2. Experimental Section

We use broadband femtosecond pump-probe microscopy to measure the ultrafast dynamics of excitons and trions in hBN-encapsulated 1L MoS₂ at low temperature (8 K). We developed a custom confocal microscope (**Figure 1**), equipped with a closed loop He cryostat, capable of transient reflectivity measurements, with high spatial and temporal resolution, as well as static reflectance contrast (RC) and photoluminescence (PL) characterizations.

For the transient measurements, we use broadband ultrashort frequency tunable visible pump and probe pulses that are delivered collinearly on the focusing objective, resulting in a

≈3 μm diameter spot on the sample. Our setup is powered by an amplified Ti:sapphire laser generating 100 fs pulses at 800 nm (1.55 eV) with 2 mJ energy and 2 kHz repetition rate. A fraction of the laser output is used to drive a noncollinear optical parametric amplifier (NOPA) pumped at 400 nm (3.1 eV) by the second harmonic of the laser, generating broadband visible pulses.^[22] The chirp of the pump pulses, mainly due to dispersive glass elements present in the setup (lenses, beam splitters, filters), is compensated by using chirped mirrors,^[23] which compress the NOPA pulses down to ≈40 fs. The pump pulses are modulated by a mechanical chopper at 250 Hz frequency. For the broadband probe pulses, a white-light continuum is generated by focusing the 800 nm output of the main laser on a 1 mm-thick sapphire plate.^[24] The probe beam is sent to a mechanical delay line which controls the delay between pump and probe pulses. We underline that the separate branches for pump and probe pulse generation provide a great flexibility in the choice of pump wavelength (tuned by the NOPA) and probe spectral window, which are completely independent. The pump and probe pulses are then collinearly combined by a thin wedged beam splitter and focused on the sample using an achromatic objective with 8 mm focal length (NA: 0.3). The sample is mounted in a closed-cycle helium cryostat reaching a temperature of 8 K. The spatial overlap of the sample with the collinear pump and probe beams is obtained by a three-axis (xyz) translation stage coupled to a home-built imaging system consisting of a white LED for the illumination and a CMOS camera (not shown) included in the optical path. In order to measure the differential reflectivity (ΔR/R) spectra, the probe beam reflected by the sample is collected by the objective lens and delivered, via an additional beam splitter, to a dispersive spectrometer with a high sensitivity CCD. The setup is also equipped with a CW 532 nm diode laser and a fiber-coupled broadband tungsten white lamp for the static optical characterization of the sample (PL and RC). For pump-probe and PL measurements, a set of long-pass and short-pass filters is used to cut out the excitation light from the signal.

The sample was fabricated using a polymethylmethacrylate (PMMA)-assisted transfer method^[25] by sandwiching a MoS₂ 1L between two thin hBN layers (45 nm bottom hBN1, 5 nm top hBN2), then placing it on a substrate. The top and bottom hBN layers provide a complete encapsulation

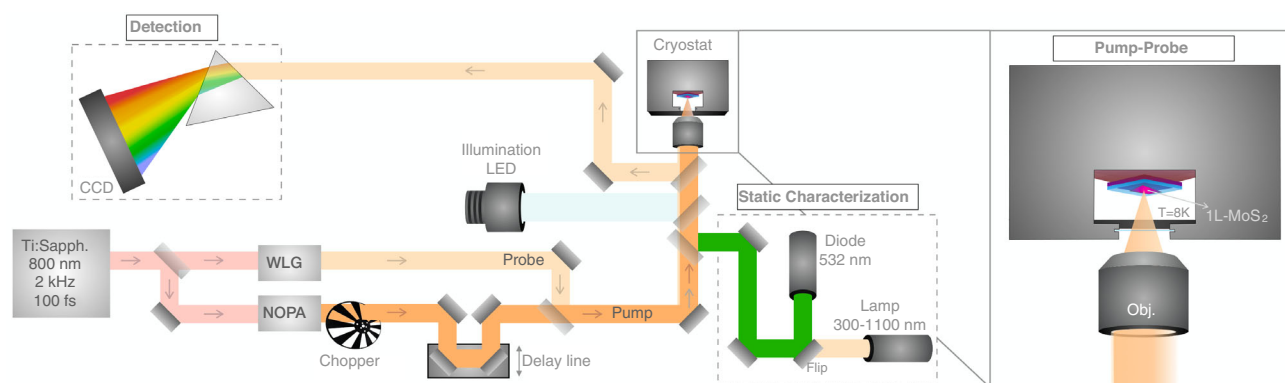


Figure 1. Sketch of the custom pump-probe microscopy setup used in our experiments. Auxiliary light sources can be coupled to the objective lens in order to perform static optical characterizations of the sample (PL and RC). Inset: Schematic view of the sample placed in a closed-loop He cryostat.

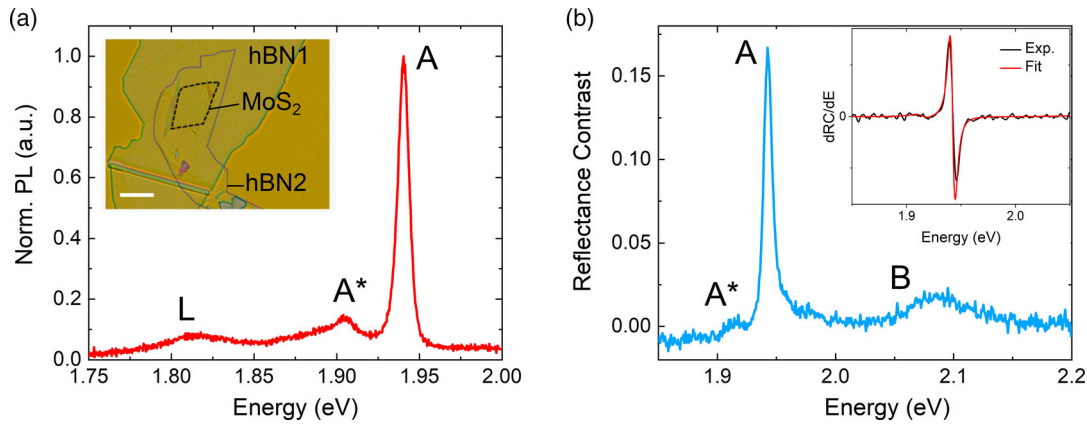


Figure 2. a) PL spectrum at 8 K of the 1 L MoS₂ excited with a CW 532 nm diode laser displaying a bright A exciton peak and weaker signals from trions (A*) and localized states (L) at lower energies. Inset: Bright-field microscope image of the 1 L MoS₂ (outlined by the black dashed line) encapsulated in hBN. Scale bar: 10 μm. b) Static RC spectrum (blue line) recorded at 8 K using a tungsten lamp, evidencing the absorption features of the neutral A and B excitons and the A* trions. Inset: Derivative of the RC spectrum (black line) fitted by a TMM model including Lorentzian oscillators (red curve).

which fully covers the area of the MoS₂ flake. Flakes of few-layers hBN and 1Ls of MoS₂ were obtained by mechanical exfoliation of bulk crystals. For the substrate, we use a dielectric mirror with a stop-band 600 meV broad and centered at 1.984 eV, terminating with a SiO₂ layer, in order to maximize the reflected probe intensity, crucial to obtain clean pump-probe measurements with a high signal-to-noise ratio. The inset of **Figure 2a** shows a bright-field microscope image of the encapsulated 1L MoS₂.

3. Results and Discussion

Figure 2a shows the PL spectrum of the encapsulated MoS₂ 1L, measured at 8 K exciting the sample with a CW 532 nm laser at 40 μW. The bright and sharp peak at 1.94 eV is related to the emission of the A excitons, observed together with a weaker peak at 1.905 eV, ascribed to emission from the trions (A*). It is worth noting that such low trion absorption/PL signal is usually observed in 1L TMDs with a modest level of natural doping.^[7] At much lower photon energies, a broad and weak peak appears in the PL spectrum, probably due to emission from localized states, labeled generically as L, generated by small residual strain or defects arising from the fabrication process.^[26]

A broadband incoherent white light source was used to measure the static RC spectrum of the encapsulated MoS₂ 1L at cryogenic temperatures (8 K), as shown in Figure 2b. The RC spectrum is calculated as $RC = (R_{\text{sub}} - R_{1L})/R_{\text{sub}}$, where R_{1L} is reflectance of the sample and R_{sub} is the reflectance taken from an area with only the two hBN layers on the substrate. In RC measurements, we clearly observe one intense and narrow peak at 1.942 eV associated with the absorption of the neutral A excitons, formed by electrons and holes in the bands minima giving the lowest energy allowed optical transition. A weaker signal related to the trion appears redshifted by about 30 meV from the A exciton. At higher energies, we observe the B excitons at 2.085 eV. In order to determine the parameters of the excitonic resonances, we model the dielectric function of the MoS₂ layer as a sum of Lorentz oscillators (one for each excitonic peak) plus a

constant ϵ_{∞} which includes all contributions lying at higher energies^[27]

$$\epsilon(\omega) = \epsilon_{\infty} + \sum_i \frac{I_i}{\omega_0^2 - \omega^2 - i\gamma_i\omega} \quad (1)$$

where I_i , $\omega_{0,i}$ and γ_i are respectively the oscillator strength, the resonance energy, and the linewidth of the i th excitonic resonance. Interference effects due to the multilayer structure strongly affect the shape of the optical response. All these effects are taken into account by the transfer-matrix method (TMM). The parameters of all the excitonic peaks are determined by fitting the first derivative of the RC spectrum. Other parameters like the thickness and refractive index of the layers composing the substrate are known and are kept fixed in the fitting procedure. We deliberately choose to fit the first derivative of the RC spectrum because the slightly sloped unintentional background of the RC spectrum is strongly suppressed by the derivative over the energy. The parameters of the fit are reported in **Table 1** for the excitonic species.

We notice that the linewidth of the neutral exciton is close to the homogeneous limit.^[11] This proves the high quality of the sample.

In order to study the temporal dynamics of excitons and trions in 1L MoS₂, we photoexcite the material with pump pulses tuned at 2.34 eV, above its bandgap. For this experiment, we set the pump fluence to 80 μJ cm⁻², below the threshold for the Mott transition.^[28] We record a differential reflectivity spectrum ($\Delta R/R = (R_{\text{pumpOn}} - R_{\text{pumpOff}})/R_{\text{pumpOff}}$) at each delay time τ , obtaining the map shown in **Figure 3a**. Immediately after time

Table 1. Fit parameters for exciton and trion species.

Fit parameters	Exciton (A)	Trion (A*)
ω_0	1.94 eV	1.91 eV
I	0.22 eV ²	0.03 eV ²
γ	7.6 meV	20 meV

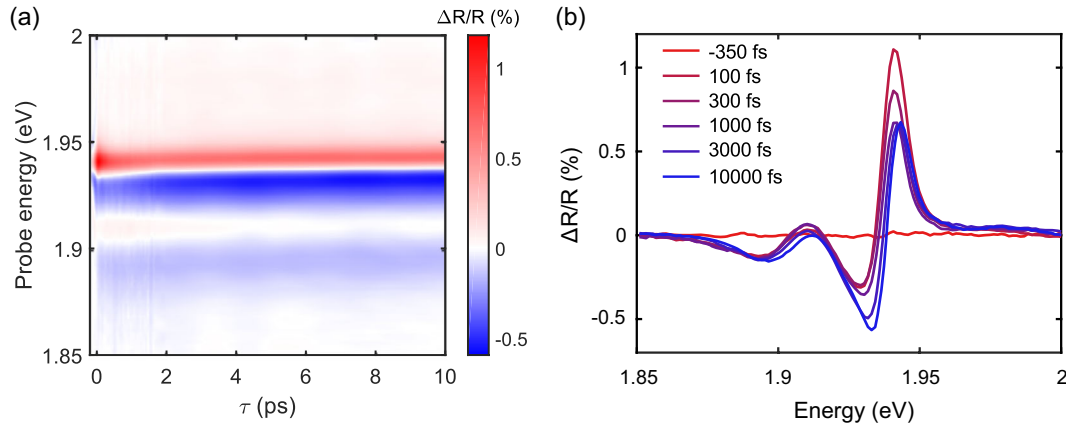


Figure 3. a) Color map of the $\Delta R/R$ signal measured on the encapsulated MoS₂ monolayer at 8 K as a function of delay time τ and probe photon energy, pumping the sample above bandgap (2.3 eV). b) Spectral cross sections of the $\Delta R/R$ map taken at different times, showing positive and negative signals in the spectral window of the A exciton and A* trion of the MoS₂ monolayer.

zero, both positive and negative signals appear in the $\Delta R/R$ map. In our experimental configuration, the positive (i.e., photobleaching) and negative features (photoinduced absorption) are attributed to pump-induced modification of the excitonic resonance (i.e., reduction of oscillator strength, broadening, and shift in energy). Figure 3b shows the spectral cross section of the $\Delta R/R$ map at different delay times, displaying how the $\Delta R/R$ spectrum changes with τ . We can clearly resolve narrow spectral features in the energy region of the A excitons and A* trions. Already after 100 fs a derivative-shaped signal appears in the spectral region of both the excitonic species, at about 1.94 and 1.91 eV. Around the A-exciton resonance, the $\Delta R/R$ signal exhibits a significant absorption bleaching (i.e., red region in the map) at small delay times, which arises from the injection of electrons and holes in the conduction and valence band, respectively, inducing absorption saturation of the excitonic transitions due to the Pauli blocking effect.^[29,30] The negative signal (i.e., blue region in the map) on the low energy side of the A exciton could be the result of the energy renormalization of the exciton due to the transient reduction of the Coulomb screening.^[31] While for A exciton the bleaching signal is very strong at all the delay times, for trions, the photoinduced absorption is predominant. This behavior can be explained considering the RC static spectrum of Figure 2b, where the trions peak is much less pronounced than that of the neutral excitons, being indicative of the low static doping in this sample, which also leads to a weaker trion bleaching signal. On the other hand, the free electron or hole carriers generated by the pump contribute to the formation of trions in the dynamic absorption spectrum, manifesting as a strong photoinduced absorption signal near the A* resonance. Recently, this effect has also been observed in encapsulated WSe₂ monolayers.^[32]

In order to extract from the $\Delta R/R$ map the temporal evolution of the A and A* peaks, we followed the procedure recently reported in ref. [33]. The transient reflectivity of MoS₂ at each delay time is determined from the equilibrium reflectivity $R(\omega)$ (which is reconstructed from the fitting parameters obtained by modeling the RC spectrum with the TMM) and the transient reflectivity map (in Figure 3) following this relation

$$R(\omega, \tau) = R(\omega) \left(\frac{\Delta R}{R}(\omega, \tau) + 1 \right) \quad (2)$$

The temporal evolution of the trion and exciton fitting parameters are then determined directly from the time-dependent reflectivity spectrum $R(\omega, \tau)$. In particular, in Figure 4a we report the temporal dynamics of oscillator strength of A and A* with respect to their value at the equilibrium ($\Delta I/I$). Neutral excitons show a very rapid formation, followed by a multiexponential decay with a fast component in the sub-ps time scale and a longer one. A zoom of the experimental A excitons dynamics up to 1.5 ps is shown in Figure 4b, together with a fitted multiexponential function convoluted with a Gaussian taking into account the instrumental response function of the apparatus. The decay times extracted from the fit are $\tau_1 \approx 133 \pm 37$ fs, $\tau_2 \approx 10.7 \pm 3.1$ ps, with an almost instantaneous rise time, in agreement with the formation dynamics previously measured in nonencapsulated MoS₂ 1L samples.^[20] In fact, it has been demonstrated that the short exciton formation timescale is the result of the ultrafast exciton cascade process upon carrier photoexcitation at high energy.^[34] The first rapid decay time (τ_1) of the A excitons can be ascribed to the combination of radiative and nonradiative direct relaxation processes of particles with small in-plane momenta which can couple to light (see the inset of Figure 4b).^[35,36] The homogeneous linewidth $\gamma = \text{FWHM}/2$ is linked to exciton lifetime T_1 through $\gamma = \hbar/T_2 = \hbar/(2*T_1) + \gamma^*$, where T_2 is the coherence time and γ^* is related to pure dephasing processes.^[37] In encapsulated TMD samples at low temperatures, the measured absorption linewidth approaches the limit of homogeneous broadening, where the coherence time is mostly dominated by the radiative lifetime of the excitonic transitions.^[12] Moreover, looking at the homogeneous linewidth of nonencapsulated 1L TMDs by performing 2D electronic spectroscopy, it has been shown that at low temperatures and small exciton densities γ^* is very small.^[38] In our case, the coherence time T_2 calculated from the absorption linewidth is $T_2 = 2\hbar/\text{FWHM} \approx 175$ fs, suggesting that the observed fast exciton decay is mostly radiative. Our measured τ_1 matches also quite well with previous theoretical calculations of the radiative lifetime for A excitons with small

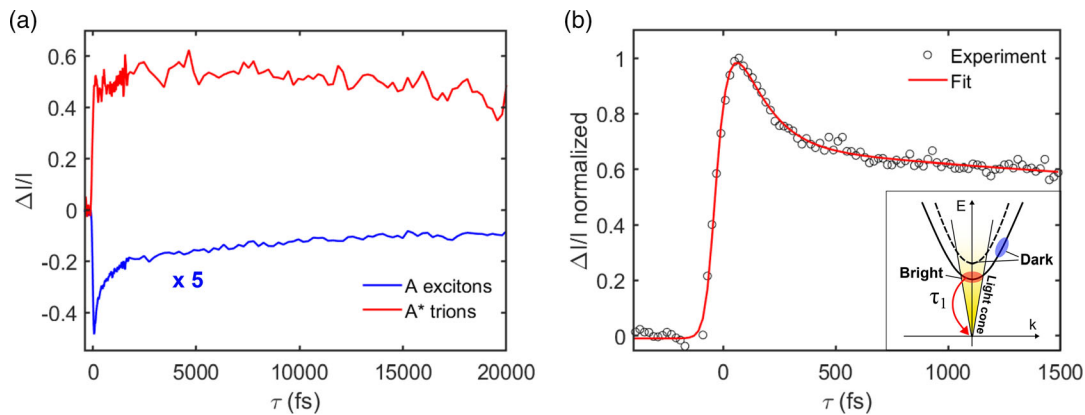


Figure 4. a) Temporal dynamics of the oscillator intensity variation of the excitonic species with respect to their value at the equilibrium ($\Delta I/I$), showing the bleaching and the photoinduced absorption for A excitons and A* trions, respectively. The A excitons trace is multiplied by a factor of 5. b) Normalized ultrafast variation of the A excitons oscillator intensity with respect to the equilibrium (black circles), fitted with a multiexponential function (red curve), shown up to 1.5 ps. Inset: Sketch of the A excitons energy-momentum dispersion showing the bright excitons recombination process (τ_1).

in-plane momenta in 1L MoS₂.^[36] The second, longer decay time of A excitons can be instead attributed to different processes related to incoherent exciton dynamics: carrier cooling from higher lying energy states at high in-plane momenta via carrier-phonon scattering^[36,39] or slow carrier recombination from dark or defect states.^[40,41]

On the other hand, photoinduced trions exhibit completely different dynamics compared to A excitons (Figure 4a). After a fast rise comparable to the build-up of A excitons, probably related to many-body effects, we observe a delayed build-up of the signal, which reaches the maximum intensity only at about 5 ps. This effect can be related to the formation dynamics of the trion.^[42] The trions decay dynamics also appear to be longer than that of the neutral excitons. This suggests that the larger Bohr radius, the lower binding energy, and the localization of the charged particles might play a major role in both the formation and recombination slow dynamics. It is well known that the excitons/trions recombination time is strongly affected by those parameters. Moreover, it has been argued that long trion formation times are also related to the small binding energy and therefore to the strength of the screened Coulomb interactions, among other factors, including excitation power, doping density, and localization length.^[42]

4. Conclusions

In summary, we measured the low-temperature (8 K) ultrafast dynamics of excitons and trions in high quality hBN-encapsulated monolayer MoS₂, with linewidths approaching the homogeneous broadening limit. We developed a custom confocal pump-probe microscopy setup to investigate samples with lateral size of few micrometers, performing transient reflectivity measurements with high spatial and temporal resolution and static optical characterizations on the same spot. We observed a very narrow linewidth of 7.5 meV for the neutral A excitons, revealing their distinct dynamics characterized by an ultrafast formation, a fast and a slow decay. We could relate the fast

exciton relaxation time to direct recombination processes, probably dominated in this sample by radiative decay. Moreover, we investigated the trions dynamics, present in the structure due to a modest natural doping, showing the predominance of photoinduced absorption in the transient reflectivity spectra and a much longer formation time compared to neutral excitons.

The rich behavior of neutral and charged excitons explored in our work offers novel insights on the many-body physics of monolayer TMDs and opens up their exploitation for fundamental studies and optoelectronic applications. Further investigations will be focused on the analysis of such encapsulated TMD monolayers embedded in gated structures,^[43] investigating the ultrafast dynamics of excitons in elevated doping regimes. In the future, the combination of our transient absorption microscope and high quality TMD samples will also enable the analysis of the ultrafast dynamics of excited Rydberg excitons.

Acknowledgements

A.G. and G.C. acknowledge support by the European Union Horizon 2020 Programme under grant agreement no. 881603 Graphene Core 3 and by the European Union Marie Skłodowska-Curie Actions (project ENOSIS H2020-MSCA-IF-2020-101029644). S.D.C. acknowledges financial support from MIUR through the PRIN 2017 Programme (Prot. 20172H2SC4). C.L. thanks the University of Sheffield for providing his Ph.D. scholarship. C.L. and A.I.T. acknowledge financial support of the European Graphene Flagship Project under grant agreement no. 881603 and EPSRC grants EP/V006975/1, EP/V026496/1, EP/V034804/1, and EP/S030751/1.

Open Access Funding provided by Politecnico di Milano within the CRUI-CARE Agreement.

Conflict of Interest

The authors declare no conflict of interest.

Data Availability Statement

The data that support the findings of this study are available from the corresponding author upon reasonable request.

Keywords

exciton dynamics, transition metal dichalcogenides, ultrafast microscopy

Received: August 5, 2022

Revised: September 21, 2022

Published online:

- [1] K. F. Mak, J. Shan, *Nat. Photonics* **2016**, *10*, 216.
- [2] K. S. Novoselov, D. Jiang, F. Schedin, T. Booth, V. Khotkevich, S. Morozov, A. K. Geim, *Proc. Natl. Acad. Sci. USA* **2005**, *102*, 10451.
- [3] G. Wang, A. Chernikov, M. M. Glazov, T. F. Heinz, X. Marie, T. Amand, B. Urbaszek, *Rev. Mod. Phys.* **2018**, *90*, 021001.
- [4] X. Xu, W. Yao, D. Xiao, T. F. Heinz, *Nat. Phys.* **2014**, *10*, 343.
- [5] M. M. Glazov, *J. Chem. Phys.* **2020**, *153*, 034703.
- [6] A. Imamoglu, O. Cotlet, R. Schmidt, *C. R. Phys.* **2021**, *22*, 89.
- [7] K. F. Mak, K. He, C. Lee, G. H. Lee, J. Hone, T. F. Heinz, J. Shan, *Nat. Mater.* **2013**, *12*, 207.
- [8] A. K. Geim, I. V. Grigorieva, *Nature* **2013**, *499*, 419.
- [9] F. Cadiz, E. Courtade, C. Robert, G. Wang, Y. Shen, H. Cai, T. Taniguchi, K. Watanabe, H. Carrere, D. Lagarde, M. Manca, T. Amand, P. Renucci, S. Tongay, X. Marie, B. Urbaszek, *Phys. Rev. X* **2017**, *7*, 021026.
- [10] J. Wierzbowski, J. Klein, F. Sigger, C. Straubinger, M. Kremser, T. Taniguchi, K. Watanabe, U. Wurstbauer, A. W. Holleitner, M. Kaniber, K. Müller, *Sci. Rep.* **2017**, *7*, 13279.
- [11] O. A. Ajayi, J. V. Ardelean, G. D. Shepard, J. Wang, A. Antony, T. Taniguchi, K. Watanabe, T. F. Heinz, S. Strauf, X. Zhu, J. C. Hone, *2D Mater.* **2017**, *4*, 031011.
- [12] M. Selig, G. Berghäuser, A. Raja, P. Nagler, C. Schüller, T. F. Heinz, T. Korn, A. Chernikov, E. Malic, A. Knorr, *Nat. Commun.* **2016**, *7*, 13279.
- [13] A. Chernikov, T. C. Berkelbach, H. M. Hill, A. Rigosi, Y. Li, O. B. Aslan, D. R. Reichman, M. S. Hybertsen, T. F. Heinz, *Phys. Rev. Lett.* **2014**, *113*, 076802.
- [14] E. M. Alexeev, D. A. Ruiz-Tijerina, M. Danovich, M. J. Hamer, D. J. Terry, P. K. Nayak, S. Ahn, S. Pak, J. Lee, J. I. Sohn, M. R. Molas, *Nature* **2019**, *567*, 81.
- [15] I. C. Gerber, E. Courtade, S. Shree, C. Robert, T. Taniguchi, K. Watanabe, A. Balocchi, P. Renucci, D. Lagarde, X. Marie, B. Urbaszek, *Phys. Rev. B* **2019**, *99*, 035443.
- [16] C. Louca, A. Genco, S. Chiavazzo, T. P. Lyons, S. Randerson, C. Trovatiello, P. Claronino, R. Jayaprakash, K. Watanabe, T. Taniguchi, S. D. Conte, arXiv preprint arXiv:2204.00485, **2022**.
- [17] G. Aivazian, H. Yu, S. Wu, J. Yan, D. G. Mandrus, D. Cobden, W. Yao, X. Xu, *2D Mater.* **2017**, *4*, 025024.
- [18] A. Singh, G. Moody, S. Wu, Y. Wu, N. J. Ghimire, J. Yan, D. G. Mandrus, X. Xu, X. Li, *Phys. Rev. Lett.* **2014**, *112*, 216804.
- [19] Z. Wang, A. Molina-Sanchez, P. Altmann, D. Sangalli, D. De Fazio, G. Soavi, U. Sassi, F. Bottegoni, F. Ciccacci, M. Finazzi, L. Wirtz, *Nano Lett.* **2018**, *18*, 6882.
- [20] C. Trovatiello, F. Katsch, N. J. Borys, M. Selig, K. Yao, R. Borrego-Varillas, F. Scotognella, I. Kriegel, A. Yan, A. Zettl, P. James Schuck, A. Knorr, G. Cerullo, S. Dal Conte, *Nat. Commun.* **2020**, *11*, 5277.
- [21] S. Dal Conte, C. Trovatiello, C. Gadermaier, G. Cerullo, *Trends Chem.* **2020**, *2*, 28.
- [22] G. Cerullo, M. Nisoli, S. Stagira, S. De Silvestri, *Opt. Lett.* **1998**, *23*, 1283.
- [23] C. Manzoni, D. Polli, G. Cerullo, *Rev. Sci. Instrum.* **2006**, *77*, 023103.
- [24] R. R. Alfano, *The Supercontinuum Laser Source: The Ultimate White Light*, Springer, New York, NY **2016**.
- [25] J. T. Mlack, P. Masih Das, G. Danda, Y.-C. Chou, C. H. Naylor, Z. Lin, N. P. López, T. Zhang, M. Terrones, A. Johnson, M. Drndić, *Sci. Rep.* **2017**, *7*, 43037.
- [26] Y. Yu, J. Dang, C. Qian, S. Sun, K. Peng, X. Xie, S. Wu, F. Song, J. Yang, S. Xiao, L. Yang, *Phys. Rev. Mater.* **2019**, *3*, 051001.
- [27] A. Raja, L. Waldecker, J. Zipfel, Y. Cho, S. Brem, J. D. Ziegler, M. Kulig, T. Taniguchi, K. Watanabe, E. Malic, T. F. Heinz, *Nat. Nanotechnol.* **2019**, *14*, 832.
- [28] A. Steinhoff, M. Florian, M. Rösner, G. Schönhoff, T. O. Wehling, F. Jahnke, *Nat. Commun.* **2017**, *8*, 1166.
- [29] F. Katsch, M. Selig, A. Knorr, *Phys. Rev. Lett.* **2020**, *124*, 257402.
- [30] V. Shahnazaryan, I. Iorsh, I. A. Shelykh, O. Kyriienko, *Phys. Rev. B* **2017**, *96*, 115409.
- [31] E. A. Pogna, M. Marsili, D. De Fazio, S. Dal Conte, C. Manzoni, D. Sangalli, D. Yoon, A. Lombardo, A. C. Ferrari, A. Marini, G. Cerullo, D. Prezzi, *ACS Nano* **2016**, *10*, 1182.
- [32] T. Y. Jeong, S.-Y. Lee, S. Jung, K. J. Yee, *Curr. Appl. Phys.* **2020**, *20*, 272.
- [33] C. Trovatiello, F. Katsch, Q. Li, X. Zhu, A. Knorr, G. Cerullo, S. Dal Conte, *Nano Lett.* **2022**, *22*, 5322.
- [34] S. Brem, M. Selig, G. Berghäuser, E. Malic, *Sci. Rep.* **2018**, *8*, 8238.
- [35] C. Robert, D. Lagarde, F. Cadiz, G. Wang, B. Lassagne, T. Amand, A. Balocchi, P. Renucci, S. Tongay, B. Urbaszek, X. Marie, *Phys. Rev. B* **2016**, *93*, 205423.
- [36] H. Wang, C. Zhang, W. Chan, C. Manolatu, S. Tiwari, F. Rana, *Phys. Rev. B* **2016**, *93*, 045407.
- [37] M. O. Scully, M. S. Zubairy, *Quantum Optics*, Cambridge University Press **1997**, <https://doi.org/10.1017/CBO9780511813993>.
- [38] G. Moody, C. Kavir Dass, K. Hao, C.-H. Chen, L.-J. Li, A. Singh, K. Tran, G. Clark, X. Xu, G. Berghäuser, E. Malic, A. Knorr, X. Li, *Nat. Commun.* **2015**, *6*, 8315.
- [39] Z. Nie, R. Long, L. Sun, C.-C. Huang, J. Zhang, Q. Xiong, D. W. Hewak, Z. Shen, O. V. Prezhdo, Z.-H. Loh, *ACS Nano* **2014**, *8*, 10931.
- [40] T. Völzer, F. Fennel, T. Korn, S. Lochbrunner, *Phys. Rev. B* **2021**, *103*, 045423.
- [41] H. Wang, C. Zhang, F. Rana, *Nano Lett.* **2015**, *15*, 339.
- [42] A. Singh, G. Moody, K. Tran, M. E. Scott, V. Overbeck, G. Berghäuser, J. Schaibley, E. J. Seifert, D. Pleskot, N. M. Gabor, J. Yan, *Phys. Rev. B* **2016**, *93*, 041401.
- [43] D. Vella, D. Ovchinnikov, N. Martino, V. Vega-Mayoral, D. Dumcenco, Y.-C. Kung, M.-R. Antognazza, A. Kis, G. Lanzani, D. Mihailovic, C. Gadermaier, *2D Mater.* **2017**, *4*, 021005.